Analyst

A low-cost, high-sensitivity 3D printed fluorescence detector

Journal:	*Analyst*
Manuscript ID	AN-ART-10-2024-001378.R1
Article Type:	Paper
Date Submitted by the Author:	17-Jan-2025
Complete List of Authors:	Snow, Robyn; The University of Memphis, Department of Chemistry Simone Jr., Paul; The University of Memphis, Department of Chemistry; Foundation Instruments, Inc. Emmert, Gary; The University of Memphis, Department of Chemistry; Foundation Instruments, Inc. Brown, Michael; The University of Memphis, Department of Chemistry; Foundation Instrument, Inc.

ARTICLE

A low-cost, high-sensitivity 3D printed fluorescence detector

Robyn A. Snow,[a] Paul S. Simone,[a,b] Gary L. Emmert,[a,b] and Michael A. Brown*[a,b]

Received 00th January 20xx,
Accepted 00th January 20xx

DOI: 10.1039/x0xx00000x

Fluorescence methods have distinct advantages over traditional absorbance methods including greater sensitivity, improved detection limits, and selectivity. Unfortunately, the cost of typical, commercially available fluorescence detectors is beyond what some industrial and research labs can afford or maintain. Having a relatively low-cost, simple to use, and high-sensitivity fluorescence detector would be very beneficial. The aim of this research is to develop a 3D printed flow through fluorescence detector that does not require complex optics or an expensive excitation source and has comparable performance to a commercial detector. The detector presented here was designed to work with nicotinamide-based methods developed in previous research; however, by simply changing the excitation and emission filters this detector can be adapted to other applications. Several evaluation studies were performed where the relative signal-to-noise ratio, detection limits, accuracy, and precision results for the 3D printed detector were compared to those of a commercial detector using nicotinamide as the analyte. Overall, the detector performed comparably or better than a commercial detector for these metrics.

Introduction

Molecular fluorescence involves the emission of photonic energy as an excited molecule (singlet state) relaxes to a lower energy state. Typical fluorescent molecules, or fluorophores, exhibit delocalized electrons and a rigid molecular structure leading to an increase in quantum yield. It is also seen that fluorescence intensity increases with decreased temperature.[1] Common fluorophores include fluorescein, quinine, rhodamine B, and coumarin. Quinine fluorescence was first observed in 1845 by Sir John Herschel, and further study of quinine in the 1950's led to the development of the first spectrofluorometer.[1-3]

Like absorption, fluorescence-based methods follow the Beer-Lambert Law, which relates the molar concentration of the fluorescing species to the fluorescence emission. As shown by Equation 1, the emission intensity (F) is directly proportional to the power of the incident beam (P_0), the pathlength (b), the molar absorptivity of the fluorescing molecule (ε), the concentration (c), the instrument parameters (K'), and the quantum efficiency (φ_f).[2]

$$F = 2.303K'\varphi_f \varepsilon bcP_0 \quad (1)$$

Assuming that b, φ_f, and ε are constant we can combine them with K' to give K'' in Equation 2 showing that fluorescence emission intensity is directly related to the molar concentration of the fluorescing species. However, the linearity of this relation is limited to low concentrations.[2]

$$F = 2.303K''c \quad (2)$$

Fluorescence methods have distinct advantages over traditional absorbance methods which include greater sensitivity, improved detection limits, and selectivity. Typical fluorescence detectors exhibit detection limits in the nanomolar range while absorbance detectors have detection limits in the millimolar range. The difference in sensitivity is attributed to the fundamental way in which the measurements are determined. Absorbance is measured as log (P_0/P), where P_0 is the initial radiant power of the light transmitted prior to interaction with a molecule and P is the radiant power of the light transmitted through the cuvette with the molecule present. Therefore, the signal measured is based on the reduction in power through absorption by the molecule. In contrast, the signal measured in fluorescence is light emitted from the interaction of the fluorophore and the excitation source photons and not directly from the excitation source.[2] Detecting the emission of light in near zero background is more effective and sensitive than detecting the reduction in light in a substantial light background. Another advantage of fluorescence is that it can add multiple levels of selectivity. For example: 1) the excitation wavelength is specific to the fluorophore; 2) the emission wavelength is specific to the fluorophore; and 3) a derivatization agent can be used to react with a non-fluorescent analyte to yield a fluorescent product that is different than the sample matrix. Ideally, this results in a measurement where the change in the fluorescent signal is due only to the fluorophore of interest. Absorption methods are not capable of discriminating between the analyte and interfering species which absorb light at the same wavelength, however fluorescent methods have the selectivity provided by excitation and emission wavelengths.

The main disadvantage of performing fluorescence measurements compared to absorbance measurements is the detector requires additional components thereby increasing the cost and complexity. The main components of an absorbance detector are the light source, the wavelength selector, the sample holder, and the photon transducer. The cost of a typical, commercially available absorbance detector can range from $500 to $6,500. A fluorescence detector requires an excitation source, two sets of filters or monochromators to select the emission and excitation wavelengths, and a photon transducer that is located orthogonally to the excitation source.[1,2] The cost of a typical,

[a]Department of Chemistry, The University of Memphis, Memphis, TN 38152, USA E-mail: mabrown@memphis.edu; Tel: +1.901.678.4427
[b]Foundation Instruments Inc., Collierville, Tennessee 38017, USA

commercially available fluorescence detector can range from $7,500 to $30,000. Unfortunately, this price point is often beyond what some industrial and research institutes can afford or maintain. Having a relatively low-cost, simple to use, and sensitive fluorescence detector would be beneficial.

When considering the construction of a low-cost fluorescence detector one must first consider the main components including the excitation source, flow-cell, optics, photon transducer, and enclosure type. The bulk of the cost for commercial fluorescence detectors is due to the complex optics, such as collimation lenses and monochromators, and the excitation source. For this research, excitation and emission filters were used in place of monochromators which resulted in a significant cost reduction. The most common excitation source for fluorescence detectors is a xenon arc lamp which produces a continuum of radiation throughout the ultraviolet-visible (UV-Vis) region (Figure S1†). Due to recent advances in LED technology, a wide range of wavelengths and radiant power options are available allowing LEDs to be a suitable option for fluorometers, fluorescence detectors, and other optical instrumentation.[4-12] Recently, LEDs capable of high-power emission in the UV region (Figure S1†) have become commercially available for less than $50, while the cost of xenon arc lamps can exceed $800. Also consider the operational lifetime of a standard xenon arc lamp is approximately 1200 hours and can burst if used past the rated lifetime. In contrast, an LED can last near 10,000 hours with less than a 20% lumen depreciation.[13,14] Therefore, for this research a UV LED was selected as the excitation source. The photon transducer of choice for most fluorescence detectors is a photomultiplier tube (PMT). While the cost of PMTs is substantially more than photodiodes and charged-coupled devices the signal-to-noise ratio is far superior, therefore a PMT was selected. A flow through quartz cell was used so that the detector could be interfaced to a chromatography or flow-injection analysis (FIA) system. To increase the simplicity, portability, and further lower the cost of the detector 3D printed components and integrated electronics were used.

Over the past decade there has been a substantial increase in the development and application of 3D printed components in analytical instrumentation. In particular, spectrophotometric systems have greatly benefited from the rapid prototyping and cost reduction provided by 3D printing technology.[15-17] Several researchers have used LEDs, photodiodes or PMTs, and 3D printed optical blocks to construct simple, low-cost absorbance and fluorescence spectrophotometers with promising results.[17-23] Some of these designs have allowed for use in flow-through applications such as FIA, HPLC, and CE[18-21] and others for manual sampling.[22,23] Other researchers have interfaced a smartphone with 3D printed optical blocks/holders for educational[24] and commercial applications.[25-27] For this research, a 3D printed fluorescence (3DFL) detector was developed and evaluated that shares similarities with previous research, however the optical block has conical light paths to eliminate the need for collimation/focusing optics and has the ability to accept normal and flow-cell type cuvettes. The 3DFL detector was built with the purpose of being used with nicotinamide chemistry which has been used extensively for the analysis of trihalomethanes (THMs)[28-30] and haloacetic acids (HAAs) though is readily adaptable for other applications.[30-34] The THMs and HAAs are the two most common classes of disinfection by-products (DBPs) produced from the chlorination of drinking water and have the potential to increase the risk of bladder and colorectal cancers[35-45] therefore are regulated by several agencies including the USEPA.[46-48] To improve the simplicity, selectivity, and sensitivity

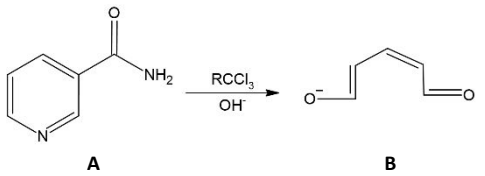

Fig. 1 The nicotinamide chemistry is based on the Fujiwara reaction. Adapted from Ranaivo et al.[50] Nicotinamide (A) reacts with the haloacetic acid (denoted as RCCl3) in heated basic solution to form fluorescent glutaconaldehyde anion (B).

of analysis of drinking water for THMs and HAAs, nicotinamide-based methods and instrumentation such as the post-column reaction ion chromatography (PCR-IC) analyzer and the capillary membrane sampling-FIA.[28-33] These methods use nicotinamide as the derivatization agent which is a fluorophore with a maximum excitation wavelength of 370 nm and a maximum emission wavelength of 455 nm. The reaction of THMs or HAAs with nicotinamide (Figure 1a) in basic solution at ~95°C for ~15 minutes to form the fluorescent product glutaconaldehyde anion (Figure 1b) is based on a modified Fujiwara reaction.[49,50] In Figure 2, a plot of relative fluorescence intensity as a function of wavelength (nm) is presented showing an overlay of the excitation and emission spectra for the nicotinamide-monobromoacetic acid product.

The main aim of this research is to develop a low-cost, flow through 3DFL detector that has comparable or better performance to that of a commercial fluorescence detector. The development and construction the "detector body" that holds the components of the detector in alignment will be discussed. In addition, the data for selection of the excitation source, excitation filter, and emission filter will be presented along with the results from detector evaluation and comparison studies using nicotinamide.

Experimental

Chemicals and Reagents

All standards were prepared in reagent grade, deionized water with a resistivity of at least 18.2 MΩ-cm and total organic carbon (TOC) of ≤ 10 µg L^{-1} produced by a Barnstead E-pure four-cartridge system (Thermo Fisher Scientific, Waltham, MA, USA). All chemicals used were reagent grade, HPLC grade, ACS Certified

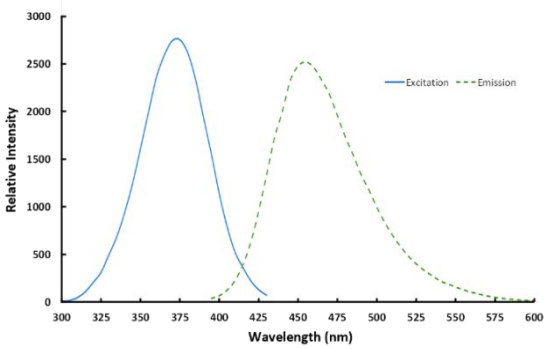

Fig. 2 Plot of the excitation spectrum (blue solid line) and emission spectrum (green dashed line) of the nicotinamide-MBAA product. The excitation spectrum shows a maximum signal at 370 nm. The emission spectrum shows a maximum signal at 455 nm.

grade of 97% or higher. The nicotinamide powder was purchased

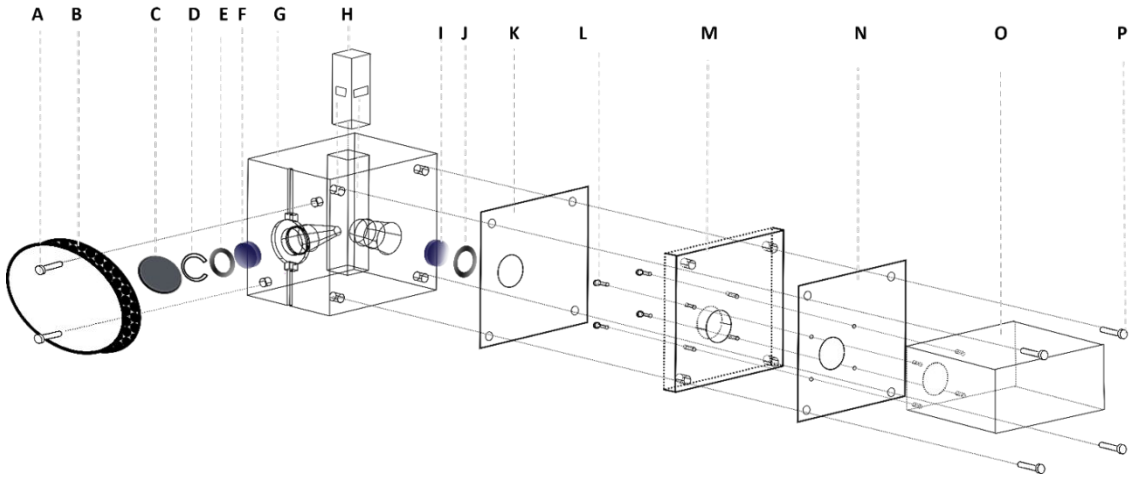

Fig. 3 Diagram of the 3DFL detector main body, PMT mount, and associated components. (A) M3 machine screws, (B) Heat sink & Fan, (C) LED mounted to MPCB, (D) inner retaining ring, (E) #7 O-ring, (F) Excitation filter, (G) 3D printed main body , (H) Flow cell, (I) Emission filter, (J) O-ring, (K) Viton light gasket, (L) M2 machine screws, (M) 3D printed PMT mount, (N) Viton light gasket, (O) PMT, and (P) M3 machine screws.

from Thermo Fisher Scientific. The stock nicotinamide standard solution was prepared by dissolving 0.0173 g of nicotinamide powder into reagent water for a total volume of 100 mL (1.42×10^{-3} M or 1417 µm). Nicotinamide standard solutions were prepared by diluting aliquots of the stock standard solution into reagent water.

Design and fabrication of the 3DFL detector

The main body of the 3DFL detector and the PMT mount were designed in TurboCAD® and printed using a Form Labs Form2® printer with black acrylonitrile butadiene styrene (ABS) resin with a z-resolution of 0.05 mm (IGES, STEP, and STL files and schematics for the 3D printed components are provided in the supplementary information document). After printing, these components were cleaned in an isopropanol bath (91% isopropanol) then dried. The detector main body (additional images Figures S2 and S3†) includes the LED housing, the mount for the optical filters, the sample flow cell, and the interface for the PMT mount The LED source and the PMT were arranged orthogonally. The excitation beam has a 0° angle of incidence. Within the main body there are two conical optical paths where one directs the LED light towards flow cell, and one directs the emitted fluorescence light towards the PMT. The conical design eliminated the need for additional collimation optics. The LED optical path contained an excitation filter and the PMT optical path contained an emission filter.

The assembly of the detector module is shown in Figure 3. The M3 EZ-Lok threaded inserts were inserted into the holes to allow mounting of the LED and PMT on the main body. The PMT was bolted to the PMT mount using M2 flat head machine screws. The PMT mount assembly was then affixed to the main body with M3 machine screws. Between the PMT mount and the main body as well as between the PMT and the mount itself are light tight gaskets made from Viton®. The excitation and emission filters were installed into the main body within the optical path and secured in place using an O-ring and an inner retaining ring. The excitation and emission filters were purchased from Edmund Optics (Edmund Optics, Barrington, NJ, USA). The excitation filter (65069) has a 12.5 mm diameter and a 5 mm thickness with a peak wavelength at 365 nm and an effective bandpass of 10 nm at full width-half maximum height (FWHM).[51] The emission filter is a longpass filter with a diameter of 12.5 mm and 2 mm thickness with a cut-on wavelength at 425 nm and a transmission wavelength range of 433 - 1650 nm.[51] The LED (Osram, LED Engin, LZ4-04UV00) has a peak emission wavelength of 365 nm with a FWHM of ~10 nm and a typical radiant flux of 3.30 W (T = 25 °C and current of 700 mA).[52] The LED was mounted directly to the main body of the detector with a heat sink and fan to dissipate the heat produced during operation. An ELDO LED driver, operated in constant current mode at 700 mA, was used to power the LED. This type of driver provides stable and flicker free operation of the LED. In addition to the LED driver, a 0 - 10 V B250K potentiometer was used to vary the intensity of the LED. A head-on PMT with a 19 mm diameter round window and response wavelength response range of 300 to 650 nm was acquired from Hamamatsu (Hamamatsu Photonics, USA, H7827-001).[53] The flow cell was from Starna (583.4.2F-Q-10/z20) and has a pathlength of 10 mm and an internal volume of 0.440 mL. Other flow cell designs and options are available from Starna and other manufacturers. The flow cell includes Teflon tubing (15.9mm outer diameter, 60 cm length) tubing for the inlet and outlet of the flow cell with M6 fittings. The inlet tubing was interfaced to the six-port injection valve (V) using 1/16" internal Valco PEEK (ZDV thread) fittings and ferrules (ZN1FPK-10; ZGF1PK-10). The optimization of the detector design eliminated the need for complex optics such as fiber optics, mirrors, or lenses. All the associated electrical components such as power supplies, LED driver, potentiometers and the 3DFL detector light tight box were housed in an aluminum enclosure.

Selection of the emission filter

Various emission filters were evaluated to achieve optimum performance. A 400 nm longpass filter (Edmund Optics, 62-974), a 450 nm center wavelength (CWL) bandpass filter (Edmund Optics, 84-770), and a 425 nm longpass filter (Edmund Optics, 65-069) were evaluated. The 400 nm longpass filter was not compatible with the nicotinamide/HAA chemistry so was omitted. The 365 nm excitation wavelength filter used for the HAA system overlapped with the 400 nm emission causing a high and erratic signal output from the PMT (Figure S4†) in the absence of nicotinamide in the flow cell. Quantifiable data was not able to be obtained with this filter. The signal from the 450 nm CWL filter was much lower than the signal from the 425 nm longpass filter; therefore, the latter filter was selected.

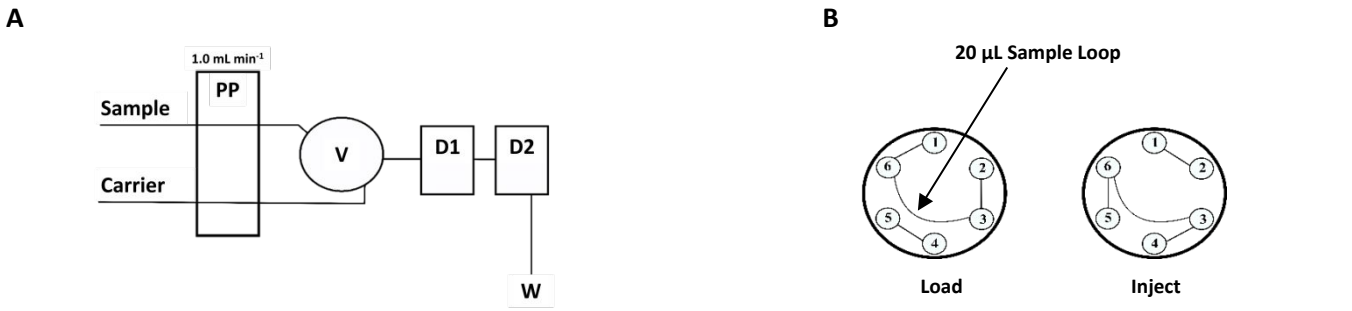

Fig. 4 (A) Block diagram of the FIA system for comparison testing of the 3DFL detector and the commercial detector. (PP) peristaltic pump set to a flowrate of 1.0 mL minute^{-1}, (V) six-port injection valve, (D1) Waters 474 FL detector, (D2) 3D printed FL detector, (W) is waste. A 20 µL sample loop was used. (B) Valve diagram showing the load and inject positions. Port 1 Sample inlet, Port 2 waste outlet, Port 3 and 6 20 µL sample loop, Port 4 carrier inlet, and Port 5 output to D1.

Flow injection instrument setup for comparison studies

A simple FIA system (Figure 4A) was assembled to compare the 3DFL detector to a commercial detector (Waters 474 dual monochromator fluorescence detector). Nicotinamide, shown in Figure 1a, was selected as the fluorescent evaluation standard and analyzed over a range of concentrations. This molecule has an excitation wavelength of 365 nm and an emission wavelength of 455 nm. The FIA system was used to control the injection and flowrate of the nicotinamide into the 3DFL detector. The system consisted of a four-channel peristaltic pump (Watson Marlow) to flow nicotinamide into a six-port electronically actuated injection valve with a 20 µL sample loop. The reagent water carrier stream was set to a flowrate of ~1.0 mL minute^{-1}. The Waters 474 detector (Comm) has an advanced optical bench comprised of grating monochromators, collimators, mirrors, and lenses. When the injection valve is in the Load position (Figure 4b), the sample stream fills the sample loop and directed out to the waste. The carrier stream flows into the valve and out to the commercial detector then through the 3DFL detector and out to waste. When the valve is actuated into the Inject position, the carrier stream flows into the valve through the sample loop to the detectors where the plug of fluorescent nicotinamide is detected as a peak.

The optimum conditions for the 3DFL detector were as follows: the voltage from the ELDO LED driver was set to 7.52 V using a potentiometer. The control voltage or gain on the PMT was set to 0.500V. The commercial detector was set to an excitation wavelength of 365 nm and an emission wavelength of 455 nm. The gain was set to 100, the attenuation was set to 8, and the response set to 3 seconds.

Results and Discussion

Comparison of the signal-to-noise ratio

Both the limit of detection (LOD) and the limit of quantitation (LOQ) are affected the noise level of the detector signal. An investigation was performed to estimate the average noise level for the 3DFL detector to offer insight about the analytical capability and limitation of the detector. The noise level was estimated from a blank run by analyzing a reagent water carrier stream by injecting an aliquot into both detectors while recording the signal for a span of two minutes. Data acquisition was performed using PeakSimple hardware (analog-to-digital converter) and integration software (SRI Instruments, California, USA). The noise level was estimated by taking the difference between the signal for the blank and the baseline by integrating each detected peak (integrated peak area, mV*s). Because the average noise level was constant there is a relative effect on the signal for analyte; as the signal of the analyte is reduced, the impact of noise upon the error associated with the measurement increases (Figure S5†). Therefore, a measurement of the signal-to-noise ratio (SNR) is a more accurate estimation of the detector's analytical capability. To obtain an estimation of the SNR, a 19.8 µM nicotinamide check standard was analyzed to estimate average signal whereas the noise was estimated by averaging 100 data points from the peak area data collected from a two-minute analysis of a reagent blank. The average peak area from *n* replicate check standards at 19.8 µM were divided by the average noise from the blank runs to obtain the representative SNR.

The results for SNR estimation for the 3DFL and commercial detectors are shown in Table 1. When comparing the noise for these detectors, consider that both the average noise in the blank and the SNR. Separately these two measurements may not provide a clear indication of the instrument performance. For example, the SNR for the two detectors varied greatly with the 3DFL detector having a SNR greater than a factor of two than the commercial detector for the same 19.8 µM nicotinamide check standard. Figure 5 shows FIA gradients of a blank and varying nicotinamide concentrations for the 3DFL detector (Figure 5A) and the commercial detector (Figure 5B). The z-axis for Figure 5B is from 15 to 18 mV, a scale much smaller than the 3DFL detector though the noise is visible. While the 3DFL detector has a higher noise level, it also has a greater increase in the signal leading to an increase in the SNR. This is further evident when comparing the method detection limit (MDL), LOQ, LOD, and the signal detection limits for the two detectors.

Table 1 Comparison of signal and noise estimates for the 3DFL detector and a commercial detector (Comm).

Type	Avg. Peak Area ChkStnd.[a]	Std. Dev. Peak Area ChkStnd.[a]	Avg. Peak Area Blank[a]	Std. Dev. Peak Area Blank[a]	SNR[b]
3DFL	$70._7$	$\pm3._5$	0.1_8	$\pm0.1_5$	$390._3$
Comm	$2._5$	$\pm0.2_0$	0.02_0	$\pm0.02_1$	$124._9$

a. Integrated peak area (mV*s)
b. Signal-to-noise ratio

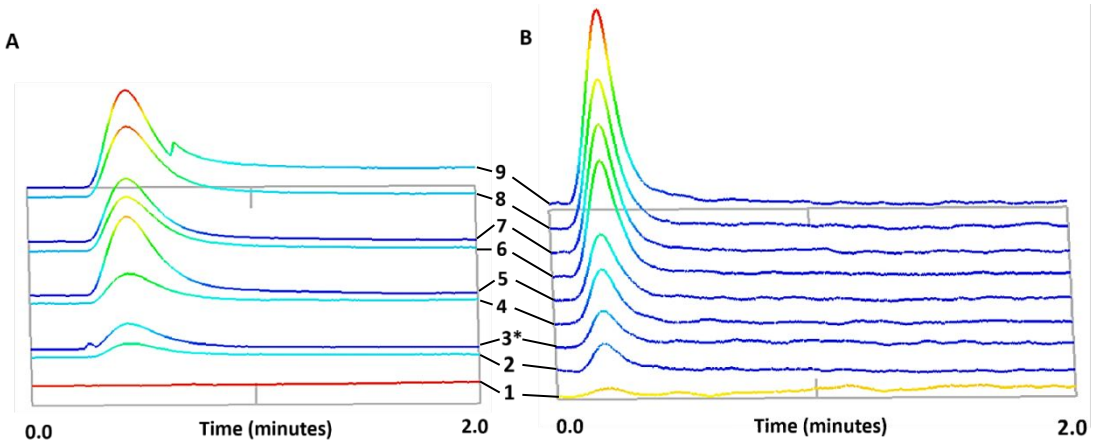

Fig. 5 Comparison of FIA gradients for a blank analysis and nicotinamide calibration standards using the (A) 3DFL detector and the (B) commercial detector. The nicotinamide calibration standards are in µM units and are shown as follows: (1) blank, (2) 1.42, (3) 19.8, (4) 34.0, (5) 48.2, (6) 70.8, (7) 90.7, (8) 104.8, and (9) 141.7. (A) 3D overlay of the nicotinamide calibration standards and blank run using the 3D printed fluorescence detector. The z-axis is the signal in mV and ranges from 73.0 to 106.0 mV. (B) 3D overlay of the nicotinamide calibration standards and blank analysis from the commercial detector. The signal range in the z-axis is from 15 to 18 mV. *Check standard

MDL, accuracy, and precision study

A MDL, accuracy, and precision study was performed using the simple FIA system as described previously with nicotinamide as the fluorescent standard with a reagent water carrier. The calibration ranged from 1.4 to 141.7 µM nicotinamide, with a check standard of 19.8 µM. The check standard was analyzed eight consecutive times. The Traditional MDL was calculated using USEPA guidelines.[54,55] The Uncertainty MDL and ISO 11843-2:2000 MDL were calculated using standard protocol.[2,56-62]

USEPA guidelines for MDL, accuracy, and precision calculation

The USEPA protocol[54,55] to determine an MDL involves first preparing a five-point calibration curve using concentrations within the expected range for the analysis. A linear regression line is then calculated from the calibration curve data, thus obtaining the slope and y-intercept and associated uncertainties. A check standard is then prepared at a concentration between the two lowest calibration points and analyzed seven consecutive times (using the same standard). The experimental concentration of the check standard is calculated by using the slope and y-intercept obtained from the linear regression. The average, standard deviation and percent recovery of the check standard experimental concentrations are calculated. The MDL (Equation 3) is calculated as the standard deviation (s) of the check standard experimental concentrations multiplied by the student's t-value at the 98% confidence interval ($t_{0.02,\,n=6}$, 3.143 for typically seven replicates).

$$\mathrm{MDL} = s * t_{0.02,\,n-1=6} \qquad (3)$$

The mean percent recovery of the seven check standards is used as a measure of the accuracy. The percent recovery of each check standard is calculated by dividing the calculated experimental concentration of the check standard by the theoretical check standard concentration and multiplying by 100. An average percent recovery of the seven check standards is calculated to obtain the mean percent recovery. The USEPA has established guidelines for acceptable accuracy ranges. When the check standard is within a factor of 2 to 5 of the MDL, the allowable accuracy is within 50 to 150%.[54,55]

The percent relative standard deviation (%RSD) is used as an estimate of the precision. The %RSD is calculated by dividing the standard deviation of the experimental check standard concentrations by the average of the check standard experimental concentrations and multiplying by 100. The USEPA established an acceptable range of %RSD to be a maximum of 30% when the check standard concentration is within a factor of two to five of the MDL.

Propagation of error MDL estimate method

The propagation of error method is based on propagating the error for a linear regression into the calculation of x.[2, 56-60] The propagated error in x, δx is shown in Equation 4:

$$\delta x = \left(\frac{s_{y/x}}{|m|}\right) * \sqrt{\frac{1}{n} + \frac{1}{N} + \frac{(y_0 - \bar{y})^2}{m^2 * \sum_i (x_i - \bar{x})^2}} \qquad (4)$$

Where $s_{y/x}$ is the standard error of the regression, n is the number of check standards, N if the number of calibration standards, m^2 is the slope of the regression line squared, y_0 is the check standard signal, $\bar{y}$ is the average of the signals from the calibration standards, and $\sum_i (x_i - \bar{x})^2$ is the sum of the squared differences from the mean in x, or S_{xx} of the calibration standards.[2,56]

Traditional MDL calculation

The traditional MDL calculation is shown in Equation 5 and is estimated by multiplying the standard error of the regression, $s_{y/x}$ by 3 and dividing by the slope of the regression line, m.

$$\text{Traditional MDL} = \frac{3 s_{y/x}}{m} \qquad (5)$$

This results in the lowest estimated concentration reportable and is often referred to as the detection limit at "three times the signal-to-noise ratio". The noise is typically measured from a blank analysis, but in the absence of a blank analysis, the standard error of the regression ($s_{y/x}$) may be used.[2,56]

Table 2 Comparison of accuracy, precision, and method detection limit results for the 3DFL detector (3DFL) and the commercial detector (Comm).

	Accuracy			Precision	MDL (µM)				Detection Limits			
Detector Type	Avg. Abs. Error (µM)[a]	% Rel. Error[b]	Mean % Rec.	%RSD	USEPA	Trad.[c]	Unc[d]	ISO	LOD[e] (µM)	LOQ[f] (µM)	Signal Detection Limit (mV*s)	Equation of Regression Line
3DFL	$2._5$	$12._6$	$112._6$	$6._1$	$4._1$	$11._0$	$6._5$	$10._0$	$4._1$	$13._5$	$10._7$	y = 2.6x + 12.9
Comm	-0.7_7	$-3._9$	$96._1$	$11._3$	$6._5$	$14._5$	$8._8$	$13._3$	$6._5$	$21._6$	0.7_6	y = 0.09x + 0.72

a. Average absolute error is calculated by subtracting the individual measured values of the check standard concentration from the theoretical concentration (19.8 µM) and average.
b. Relative error is calculated by dividing the absolute error by the theoretical concentration of the check standard (19.8 µM) and multiplying by 100.
c. Traditional method for calculation of the MDL using regression error
d. Uncertainty method for calculation of the MDL using propagated uncertainty equation for linear regression
e. Limit of detection
f. Limit of quantitation

ISO (ISO 11843-2:2000, ISO, Geneva) MDL calculation

The ISO MDL calculation[61] is based on the calibration data and is said to be "more statistically defensible".[62] The ISO MDL is calculated as shown in Equation 6:

$$\mathrm{MDL} = \frac{2t_{0.05,n-2}s_{y/x}}{m}\sqrt{\frac{1}{K}+\frac{1}{I*J}+\frac{\bar{x}^2}{J\sum_i (x_i-\bar{x})^2}} \quad (6)$$

Where $t_{0.05,n\text{-}2}$ is the t-statistic at the 95% confidence level, $s_{y/x}$ is the estimate of the standard error of the regression, m is the slope of the regression line, K is the number of replicate check standards, I is the total number of calibration standards, J is the number of replicates (if any) that each calibration standard was run, $\bar{x}$ is the average concentration of the calibration standards, and x_i is the individual concentration of each calibration standard.[61,62] The ISO MDL calculation often results in the largest calculated MDLs.

Summary of MDL, accuracy, and precision results

The results of the MDL, accuracy and precision study are presented in Table 2 as well as a comparison of the LOD, LOQ and signal detection limit. The LOD, LOQ and signal detection limit are calculated as follows in Equations 7 and 8.

$$\mathrm{LOD} = \frac{3s}{m} \quad (7)$$

$$\mathrm{LOQ} = \frac{10s}{m} \quad (8)$$

Where s is the standard deviation of the check standard (this is a good estimate for the noise level if the check standard concentration is near the detection limit) and m is the slope of the regression line from the calibration (a good estimate of sensitivity). The LOD is the minimum detectable concentration of analyte that is significantly different from the blank signal.[56] The LOQ is the minimum amount that can be measured with acceptable accuracy.[56] The signal detection limit (Equation 9), y_{dl}, is calculated by adding three times the standard deviation of the check standards ($3s$) to the average noise from the blank run (y_{blank}). The signal detection limit or minimum detectable signal is the minimum peak area that can be distinguished from the noise.[56]

$$y_{dl} = y_{blank} + 3s \quad (9)$$

The results of the MDL, accuracy and precision study, and the LOD, LOQ and signal detection limits for each detector are presented in Table 2. The slope of a calibration curve is the change in signal per unit concentration and is typically a good indicator of the sensitivity of the instrument and/or method. The more sensitive the detector, the greater the change in analytical signal will be observed for increases in concentration. The slope of the regression line for the commercial detector is 0.09, while the 3DFL detector has a slope of 2.6. This would suggest that the 3DFL detector has better sensitivity than the commercial detector. Two main factors could be responsible for this difference in slope. First, the volume of the flow cells is significantly different. The commercial detector had a flow cell volume of 16 µL and the 3DFL detector 0.440 mL (440 µL). This difference leads to an increase in the amount of excitation light interacting with the sample, in turn, causing an increase in sensitivity. One drawback with having a larger flow cell volume is an increase in band broadening. It was observed when the 3DFL detector was placed in front of the commercial detector the band broadening for the commercial detector was great enough to reduce the peak area for nicotinamide to near zero. A second factor to consider was the amount of fluorescence photons reaching the PMT in each detector was different. The 3DFL detector uses a 425 nm longpass filter while the commercial detector used a monochromator with a grating with a bandwidth of ~40 nm. Additional fluorescence photons can pass through the 425 nm longpass filter compared to the grating. This can help to improve sensitivity though can lead to an increase in the noise level. This is evident when the signal detection limits (peak area, mV*s) are compared for both detectors. The signal detection limit (SDL) for the commercial detector was 0.7_6 mV*s and the 3DFL detector was $10._7$ mV*s. This data suggests that the commercial detector can distinguish a smaller change in peak area relative to the noise level compared to the 3DFL detector though is less sensitive to changes in nicotinamide concentration.

The 3DFL detector exhibits lower MDL values for nicotinamide for all calculations when compared to the commercial detector. The MDLs for the 3DFL detector ranged from $4._1$ to $11._0$ µM and for the commercial $6._5$ to $14._5$ µM. The lower detection limits of the 3DFL detector are most likely a direct result of the increase in sensitivity of this detector. The precision, measured as %RSD, for the 3DFL detector was $6._1$%, and the commercial detector was at $11._3$%. The detectors both operate within acceptable accuracy the accuracy of the commercial detector is 96% and the 3DFL detector 113%.[54] While the 3DFL detector has a higher noise level, indicated in the average peak noise in the blank run, the SNR is high enough such that this noise is insignificant for a 19.8 µM check standard concentration. In such cases where the check standard is greater than a factor of five larger than the USEPA MDL, another USEPA MDL study is typically conducted. In this case, the check standard concentration is within a factor ~4 – 5, and further reduction of the check standard concentration resulted in the non-linear

region of the fluorescence emission. This complicates the MDL, accuracy, and precision study using linear regression. Further, all four detection limit estimates agree indicating that a good estimate of the detection limit is in the range of ~4 – 11 µM. The commercial detector, having a much lower SNR comparatively, exhibits a larger %RSD than that of the 3DFL detector at this check standard concentration, there is more "scatter" in the reported concentration. The percentage of noise relative to the signal of the check standard for the commercial detector is ~0.8%. While this a small fraction, when compared to the same value for the 3DFL detector of ~0.3%, it helps to explain why the %RSD is lower for the 3DFL detector. There is a trade-off for the higher sensitivity and SNR of the 3DFL detector with the noise. This is seen in the comparison data between the commercial detector and the 3DFL detector as the 3DFL detector has a larger SNR, yet the MDLs are comparable to that of the commercial detector. At the noise level this is to be expected as larger SNR offer minimal improvement.

Conclusions

A simple 3D printed fluorescence detector was successfully developed and a side-by-side comparison with a commercially available detector was performed. The metrics used to gauge the performance of the detectors were the SNR, LOD, LOQ, signal detection limit, MDL, accuracy, and precision. Using nicotinamide as a test analyte, the 3DFL detector demonstrated comparable performance to that of the commercial detector. The 3DFL detector uses no complex optics such as mirrors or lenses, and therefore costs much less to build. In addition, there is never a need to align the lamp because the flow cell, once inserted, is already aligned with the light from the excitation source. The 3DFL detector will be able to be used in place of a commercial detector for use with methods that rely on nicotinamide chemistry and can easily be adapted for other fluorescence detection method by simply changing the excitation and emission filters.

Author contributions

Snow and Emmert conceived the initial 3D printed fluorescence detector concept and design with subsequent design improvements made by Snow with input by all authors. Snow performed all experiments, data collection and interpretation and prepared the initial manuscript. The final manuscript was written and edited through the contributions of all authors.

Conflicts of interest

Gary L. Emmert, Paul S. Simone, and Michael A. Brown are part-time employees/owners of Foundation Instruments, Inc. The SBIR Phase II NSF Grant #1556127 awarded funds to Foundation Instruments, Inc. to develop products such as the 3DFL detector. The 3DFL detector is used in patented technology and commercial instrumentation.

Data availability

The data supporting this article has been included as part of the Supplementary Information document including 3D model files for the main optical block. Certain data pertaining to patented technology development was not provided as it is proprietary information.

Acknowledgements

The authors are grateful to Foundation Instruments, Inc. for funding portions of this research and permission to use their 3D-printing facility and machine shop. This material is based upon work supported by supported by National Science Foundation under SBIR Phase II NSF Grant #1556127.

References

1 J. R. Lakowicz, Ed., *Principles of Fluorescence Spectroscopy*, Springer US, Boston, MA, 2006.
2 D. A. Skoog, F. J. Holler and S. R. Crouch, *Principles of Instrumental Analysis*, Cengage Learning, Belmont, CA, 6th edition., 2006.
3 P. C. DeRose, *Recommendations and Guidelines for Standardization of Fluorescence Spectroscopy*, National Institute of Standards and Technology, Gaithersburg, MD, 1st edition., 2007.
4 D. C. Mukunda, V. K. Joshi and K. K. Mahato, *Appl. Spectrosc. Rev.*, 2022, **57**, 1–38.
5 H. Ji, M. Li, L. Guo, H. Yuan, C. Wang and D. Xiao, *Electrophoresis*, 2013, **34**, 2546–2552.
6 Y. Li, M. Dvořák, P. N. Nesterenko, N. Nuchtavorn and M. Macka, *Sensors and Actuators B: Chemical*, 2018, **255**, 1238–1243.
7 D. Xiao, S. Zhao, H. Yuan and X. Yang, *Electrophoresis*, 2007, **28**, 233–242.
8 M.-H. Sorouraddin, M. Saadati and H. K. Baneshat, *Sensors and Actuators B: Chemical*, 2013, **188**, 73–77.
9 X. Geng, D. Wu and Y. Guan, *Talanta*, 2012, **88**, 463–467.
10 S. Casado-Terrones, J. F. Fernández-Sánchez, A. Segura-Carretero and A. Fernández-Gutiérrez, *Anal. Biochem.*, 2007, **365**, 82–90.
11 B. Yang, M. C. Patsavas, R. H. Byrne and J. Ma, *Marine Chem.*, 2014, **160**, 75–81.
12 K. M. G. de Lima, *Microchem. J.*, 2012, **103**, 62–67.
13 USHIO, USHIO Xenon Short arc UXL Specifications, https://www.ushio.com/product/xenon-short-arc-uxl/, (accessed July 23, 2019).
14 DOE, Lifetime of White LEDs, https://betterbuildingssolutioncenter.energy.gov/sites/default/files/attachments/lifetime_white_leds.pdf, (accessed July 1, 2024).
15 A. Ambrosi and A. Bonanni, *Mikrochim. Acta*, 2021, **188**, 265.
16 E. J. Carrasco-Correa, E. F. Simó-Alfonso, J. M. Herrero-Martínez and M. Miró, *TrAC Trends Anal. Chem.*, 2021, **136**, 116177.
17 B. Gross, S. Y. Lockwood and D. M. Spence, *Anal. Chem.*, 2017, **89**, 57–70.
18 J. Prikryl and F. Foret, *Anal. Chem.*, 2014, **86**, 11951–11956.
19 L. D. Casto, K. B. Do and C. A. Baker, *Anal. Chem.*, 2019, **91**, 9451–9457.
20 M. Michalec and Ł. Tymecki, *Talanta*, 2018, **190**, 423–428.
21 M. Michalec, R. Koncki and Ł. Tymecki, *Talanta*, 2019, **198**, 169–178.
22 Y.-H. Shin, M. T. Gutierrez-Wing and J.-W. Choi, *Micro Nano Syst. Lett.*, 2018, **6**, 16.
23 Y. Wang, Z. Zeng, L. Yang, H. Zeng, Y. Li, Q. Pu and M. Zhang, *Anal. Chem.*, 2023, **95**, 2146–2151.
24 L. G. Pap and J. A. Stratton, *J. Chem. Educ.*, 2024, **101**, 5395–5401.

25 D. Shamsaei, S.-A. Hsieh, I. Ocaña-Rios, S. J. Ryan and J. L. Anderson, *Anal. Chim. Acta*, 2023, **1280**, 341863.
26 M. Granica and Ł. Tymecki, *Talanta*, 2019, **197**, 319–325.
27 L. Khoshmaram, M. Mohammadi and A. Nazemi Babadi, *Microchem. J.*, 2021, **171**, 106773.
28 T. Aoki and K. Kawakami, *Water Res.*, 1989, **23**, 739–742.
29 G. Geme, M. Brown, P. Simone and G. Emmert, *Water Res.*, 2005, **39**, 3827–36.
30 G. Emmert, G. Geme, M. Brown and P. Simone, *Anal. Chim. Acta*, 2009, **656**, 1–7.
31 P. Simone, G. Anderson and G. Emmert, *Anal. Chim. Acta*, 2006, **570**, 259–66.
32 P. Simone, P. Ranaivo, G. Geme, M. Brown and G. Emmert, *Anal. Chim. Acta*, 2009, **654**, 133–40.
33 P. Ranaivo, C. Henson, P. Simone and G. Emmert, *Anal. Methods*, 2011, **3**, 2873–2880.
34 C. Henson, G. Emmert and P. Simone, *Chemosphere*, 2014, **117C**, 586–595.
35 S. W. Krasner, H. S. Weinberg, S. D. Richardson, S. J. Pastor, R. Chinn, M. J. Sclimenti, G. D. Onstad and A. D. Thruston, *Environ. Sci. Technol.*, 2006, **40**, 7175–7185.
36 S. D. Richardson, M. J. Plewa, E. D. Wagner, R. Schoeny and D. M. Demarini, *Mutat. Res.*, 2007, **636**, 178–242.
37 S. Hrudey and J. Fawell, *Water Sci. & Tech.: Water Supply*, 2015, **15**, 667.
39 J. C. Coffin, R. Ge, S. Yang, P. M. Kramer, L. Tao and M. A. Pereira, *Toxicol. Sci.*, 2000, **58**, 243–252.
40 C. M. Villanueva, K. P. Cantor, J. O. Grimalt, N. Malats, D. Silverman, A. Tardon, R. Garcia-Closas, C. Serra, A. Carrato, G. Castaño-Vinyals, R. Marcos, N. Rothman, F. X. Real, M. Dosemeci and M. Kogevinas, *Am. J. Epidemiol.*, 2007, **165**, 148–156.
41 M. Kajino and M. Yagi, in *Hydrocarbons and Halogenated Hydrocarbons in the Aquatic Environment*, eds. B. K. Afghan, D. Mackay, H. E. Braun, A. S. Y. Chau, J. Lawrence, D. R. S. Lean, O. Meresz, J. R. W. Miles, R. C. Pierce, G. A. V. Rees, R. E. White, D. M. Whittle and D. T. Williams, Springer US, Boston, MA, 1980, pp. 491–501.
42 D. Stalter, E. O'Malley, U. von Gunten and B. I. Escher, *Water Res.*, 2016, **91**, 19–30.
43 National Toxicology Program, *Report on Carcinogens Monograph on Haloacetic Acids Found as Water Disinfection By-Products: RoC Monograph 12*, National Toxicology Program, Research Triangle Park (NC), 2018.
44 J. A. Pals, J. K. Ang, E. D. Wagner and M. J. Plewa, *Environ. Sci. Technol.*, 2011, **45**, 5791–5797.
45 E. Cemeli, E. D. Wagner, D. Anderson, S. D. Richardson and M. J. Plewa, *Environ. Sci. Technol.*, 2006, **40**, 1878–1883.
46 USEPA, National Primary Drinking Water Regulations: Disinfectants and Disinfection By-products Rule, (1998).
47 USEPA, Stage 1 and Stage 2 Disinfectants and Disinfection Byproducts Rules, https://www.epa.gov/dwreginfo/stage-1-and-stage-2-disinfectants-and-disinfection-byproducts-rules, (accessed September 4, 2024).
48 USEPA, Diving Into Regulations, https://www.epa.gov/dwreginfo/diving-regulations, (accessed September 4, 2024).
49 M. S. Moss and H. J. Rylance, *Nature*, 1966, **210**, 945–946.
50 P. Ranaivo, Dissertation, The University of Memphis, 2011.
51 Edmund Optics, Edmund Optics: Optical Filters-Bandpass filters, https://www.edmundoptics.com/c/bandpass-filters/617/, (accessed September 2, 2024).
52 OSRAM, LED Engin, LZ4-04UV00 product file, http://www.ledengin.com/files/products/LZ4/LZ4-04UV00, (accessed August 30, 2019).
53 Hamamatsu, Photomultiplier tube module H7827-001, https://www.hamamatsu.com/eu/en/product/optical-sensors/pmt/pmt-module/voltage-output-type/H7827-001.html, (accessed August 30, 2024).
54 P. S. Fair, C. A. Madding, D. J. Munch and R. K. Sorrell, DBP/ICR Analytical Methods Manual, EPA 814-B-96-002, 1996a. | NEPIS | US EPA, https://nepis.epa.gov (accessed September 3, 2024).
55 USEPA, Method 552.3 Determination of Haloacetic Acids and Dalapon in Drinking Water by Liquid-Liquid Microextraction, Derivatization, and Gas Chromatography with Electron Capture DetectionDocument Display | NEPIS | US EPA, https://nepis.epa.gov (accessed September 4, 2024).
56 D. C. Harris, *Quantitative Chemical Analysis*, W. H. Freeman, New York, NY, 9th edition., 2015.
57 M. A. Brown and G. L. Emmert, *Anal. Chim. Acta*, 2006, **555**, 75–83.
58 G. L. Emmert, M. A. Brown, Z. Liao, G. Cao and C. Duty, *Anal. Chim. Acta*, 2006, **560**, 197–206.
59 M. A. Brown, S. Miller and G. L. Emmert, *Anal. Chim. Acta*, 2007, **592**, 154–161.
60 A. W. Brown, P. S. Simone, J. C. York and G. L. Emmert, *Anal. Chim. Acta*, 2015, **853**, 351–359.
61 ISO, ISO 11843-2:2000 Capability of detection Part 2: Methodology in the linear calibration case, https://www.iso.org/standard/20186.html.
62 D. B. Hibbert and J. J. Gooding, *Data Analysis for Chemistry: An Introductory Guide for Students and Laboratory Scientists*, Oxford University Press, New York, 1st edition., 2005.

Data availability

The data supporting this article has been included as part of the Supplementary Information document. Certain proprietary information concerning detector block designs has not been included.